

Degradation of Endocrine Disruptors using Modified TiO₂ Nanorods under Sunlight

Radhika.S, Jesty Thomas*

Department of Chemistry, Kuriakose Elias College, Mannanam, Kottayam, Kerala, India

ABSTRACT

Anatase phase TiO₂ nanorods modified with perylene nanoparticles (PeNPs) (PNR₅₂₀) showing excellent photocatalytic activity under sunlight were synthesized. Titanium isopropoxide [C₁₂H₂₈O₄Ti] and aqueous KOH solution were hydrothermally treated to form hydrogen titanate and were calcined at 520°C to get TiO₂ nanorods. PeNPs were prepared from perylene-3,4,9,10-tetracarboxylic dianhydride using D-glucosamine hydrochloride. Phase transition from hydrogen titanate to pure anatase phase TiO₂ was confirmed by X-ray diffraction analysis. high resolution transmission electron microscopic analysis shows that the anatase phase TiO₂ consists of nanorods. Photocatalytic activities of the samples were assessed by studying the photocatalytic degradation of rhodamine B. Study reveals that TiO₂ nanorods modified with PeNPs could completely degrade common endocrine disruptors such as 4-chlorophenol, resorcinol, and salicylic acid under sunlight and are more efficient than the commercial photocatalyst Degussa P25.

Key words: Anatase TiO₂, Perylene nanoparticles, Pollutant degradation, Solar photocatalyst.

1. INTRODUCTION

Significant attention has been gained by researches focusing on the remediation of endocrine disrupting compounds as they have an adverse impact on living organisms and environment [1]. Endocrine disrupting chemicals are exogenous agents which interfere with the synthesis, secretion, transport, binding, and elimination of natural hormones in the body that is responsible for the maintenance of homeostasis, reproduction, development, and behavior [2]. They mimic the actions of natural hormones present in living organisms, causing genetic disorders such as tumors and infertility. Phenolic compounds such as chlorophenols, resorcinol (R), and phenolic acids belong to the category of endocrine disruptors. 4-chlorophenol (4-CP), R, and salicylic acid (SA) are usually found in the wastewaters of paper, pharmaceutical, and dyestuff industries [3,4]. Phenolic compounds discharged from these sources may result in the widespread contamination of the aquatic ecosystem due to their hazardous and carcinogenic properties. Hence, they are considered as persistent, bioaccumulative, and toxic (PBT) chemicals by the US Environmental Protection Agency. Remediation of PBT chemicals is a serious issue as they are very difficult to degrade using conventional treatment methods.

Semiconductor photocatalysis is a novel green technology for the complete mineralization of PBT chemicals. TiO₂ is an extensively used photocatalysts for this purpose because of its properties such as non-toxicity, inertness (chemically and biologically), and photocatalytic stability [5]. It is widely regarded that ultra-fine catalyst powders with high surface area and crystallinity are desirable to enhance the photocatalytic activity [6]. Recycling and maintaining high activity of photocatalysts are critical issues toward long-term photocatalytic applications. In practical photocatalytic process, separation of these fine powder photocatalysts from solution after the reaction is very difficult; also the tendency to agglomerate into larger particles reduces the photocatalytic efficiency during reuse [7]. One (1D) dimensional systems, such as nanowires and nanorods, are the small dimension

structures which can be used for the efficient transport of charge carriers and optical excitations. They can be easily recovered from reaction mixture than nanopowders [8,9]. Among different kinds of TiO₂ nanostructures, nanorods/tube based materials are promising in various fields such as dye sensitive solar cells [10], photocatalysts [11], and medical field [12] ascribed to the characteristic features of these 1D nanostructures. In this study, we have synthesized anatase phase TiO₂ nanorods for photocatalysis, through simple hydrothermal route, followed by calcination without using any templates.

Anatase TiO₂ having a large band gap of 3.2 eV, limits its applications utilizing the visible region, which consists of 45% of solar spectrum. Significant efforts have been devoted to enhancing the efficiency of TiO₂ under visible light using various methods such as metal/non-metal doping [1,3], formation of hetero structures with organic dyes, and photosensitive molecules [13]. Sensitization of wide band gap semiconductors using photosensitive molecules is an efficient method for expanding the absorption to visible region to exploit solar light for photocatalysis. The photosensitive molecules act as an antenna which captures the energy of sunlight and initiates the ultrafast electron injection from the singlet excited state of the photosensitive molecule into the conduction band (CB) of the semiconductor in femtoseconds [14].

Organic dye nanoparticles such as perylene nanoparticles (PeNPs) exhibit distinctive optoelectronic properties superior to their bulk

*Corresponding author:

E-mail: jestyk@kecollege.ac.in

ISSN NO: 2320-0898 (p); 2320-0928 (e)

DOI: 10.22607/IJACS.2020.804003

Received: 08th August 2020

Revised: 23rd August 2020

Accepted: 28th November 2020

counter parts, and they are of significant use in areas such as biolabeling, novel luminescent materials, non-linear optics, and chemical sensors [15,16]. Thus, they are expected to have higher photosensitization of TiO_2 . However, to the best of our knowledge, the enhancement of photocatalytic efficiency of TiO_2 by photosensitive organic nanoparticles is seldom reported. Nevertheless, the applications of PeNPs in photocatalysis are limited probably due to the poor stability in water [16,17]. Hence, we used an innovative method to synthesize stable PeNPs from perylene-3,4,9,10-tetracarboxylic dianhydride (PTCDA) using D-glucosamine hydrochloride (GAH) which acts both as reducing and stabilizing agent. The as-prepared PeNPs are incorporated into pure anatase phase TiO_2 nanorods (PNR₅₂₀), and the resulting TiO_2 -based nanocomposites showed greatly enhanced photocatalytic activity under solar light as compared to those of bare TiO_2 and most active photocatalyst, Degussa P25.

2. EXPERIMENTAL

2.1. Materials and Methods

Analytical grade titanium (IV) isopropoxide [TIP, $\text{Ti}(\text{OC}_3\text{H}_7)_4$], [PTCDA, $\text{C}_{24}\text{H}_8\text{O}_6$], [GAH, $\text{C}_6\text{H}_{14}\text{ClNO}_5$], rhodamine B [RhB, $\text{C}_{28}\text{H}_{31}\text{ClN}_2\text{O}_3$], and R ($\text{C}_6\text{H}_6\text{O}_2$) were purchased from Sigma-Aldrich chemicals. Potassium hydroxide (KOH), (4-CP, $\text{C}_6\text{H}_5\text{OCl}$), and (SA, $\text{C}_7\text{H}_6\text{O}_3$) were purchased from Merck (India). All chemicals were used without further purification. Deionized water was used throughout the experiments.

2.2. Experimental Procedure

2.2.1. Synthesis of PeNPs

PeNPs for sensitization of TiO_2 were synthesized in a single step from PTCDA by chemical reduction technique employing a biologically active molecule GAH [18]. 1 ml solution of PTCDA in acetone (1.3 mM) was injected by a micro syringe into 30 ml of GAH aqueous solution (25 mM) with vigorous stirring at room temperature. The mixture was stirred well to disperse the PeNPs in water. The formation of PeNPs was identified by the development of fluorescent yellow color and was confirmed by ultra violet (UV)-visible absorption spectra and fluorescence spectra.

2.2.2. Synthesis of TiO_2 photocatalysts

3.0 ml of TIP was pipetted into a clean dry beaker and 18.0 M KOH was added with stirring until the formation of white precipitate was ceased. The precipitate was stirred well for overnight and was transferred into stainless steel Teflon lined autoclave and the reaction proceeded at 150°C for 48 h. After the completion of autoclave treatment, it was allowed to cool down at room temperature. The precipitate was filtered, washed with deionized H_2O followed by very dil. HCl till pH 7.0 is obtained. Finally, the precipitate was washed with acetone and dried at 80°C to get hydrogen titanate and is designated as HT. HT was calcinated at 420°C and 520°C for 4 h and the products were designated as HT₄₂₀ and NR₅₂₀, respectively. Figure 1 shows the diagrammatic representation of synthesis of photocatalysts.

2.2.3. Synthesis of TiO_2 photocatalysts modified with PeNPs

The sample, NR₅₂₀ (0.2 g) was dispersed in the as prepared PeNPs. To this 20 ml of deionized water was added and the mixture was stirred well for 60 min and dried to get TiO_2 modified with PeNPs which is designated as PNR₅₂₀.

2.3. Characterizations

X-ray diffraction patterns (XRD) of the synthesized samples were obtained on a Rigaku Miniflex 600 diffractometer using $\text{Cu K}\alpha$ ($\lambda=0.15418$ nm) radiation in the range of 20° – 60° . Fourier-transform infrared (FT-IR) spectra were analyzed in a Bruker Alpha FT-IR/

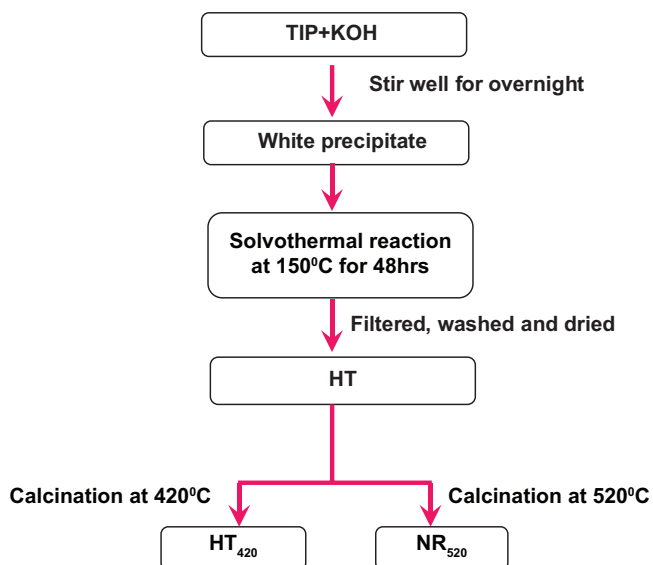


Figure 1: Schematic diagram for the synthesis of photocatalysts.

NIR Spectrometer. Photoluminescence emission (PL) spectral measurements were made using spectrofluorophotometer SL174 at an excitation wavelength of 300 nm using 150W Xenon lamp as excitation source. The high resolution transmission electron microscopic (HR-TEM) image of the sample was obtained on a JEOL JEM-2100 field emission electron microscope. Diffuse reflectance spectra of the samples were analyzed using Jasco V-770 spectrophotometer.

2.4. Photocatalytic Activity Study

Photocatalytic activity was measured with Heber solar simulator (Heber Scientific, model no: H MV-88123) which consists of tungsten halogen lamp (as visible light source) and mercury vapor lamp (as UV light source) along with A.M 1.5G filter. A.M 1.5G gives a standard solar spectrum measured on earth. Photocatalytic activity of the synthesized samples was assessed by studying the photocatalytic degradation of RhB dye. For a typical photocatalytic experiment, 0.03 g of the synthesized sample was suspended in 25 ml of 15 ppm RhB aqueous solution. The resulting suspension was equilibrated by stirring in the dark for 30 min. To study the photocatalytic degradation under sunlight, RhB-photocatalyst suspension was kept under solar irradiation at room temperature. The samples were withdrawn at different time intervals and centrifuged at 6000 r.p.m. to separate the photocatalyst. The absorbance of RhB was measured at 553 nm using a Systronics 2203 double beam spectrophotometer. It was observed that no detectable degradation of RhB occurs without photocatalyst or solar irradiation alone. Further, the catalyst was applied for the degradation of model endocrine disruptor phenolic compounds such as (4-CP, 20 ml of 30 ppm), (R, 20 ml of 30 ppm), and (SA, 20 ml of 100 ppm) under sunlight. The photocatalytic degradation of 4-CP, Rm and SA was studied by measuring the absorbance at 280, 274, and 302 nm, respectively, using a UV-vis spectrophotometer. The presence of active radical species and their role on photocatalysis was tested by trapping the active species using some sacrificial agents. Isopropyl alcohol (IPA), ascorbic acid (AA), and triethanolamine (TEOA) were used as hydroxyl free radical ($\cdot\text{OH}$), superoxide anion radical ($\cdot\text{O}_2^-$), and hole (h^+) scavenger, respectively. The experimental procedure involves the addition of 1mM of scavengers to photocatalyst-dye solution (0.03 g, 25 ml of 15 ppm RhB). The mixture was then exposed to solar irradiation and the changes in the concentration of RhB were monitored at 553 nm.

3. RESULTS AND DISCUSSION

The mechanism of formation and characterization of PeNPs is previously reported by our group [18]. UV-vis absorption spectra of PTCDA-GAH solution at different reaction time intervals confirmed the formation of PeNPs. There was a decrease in intensity of UV region peak (265 nm) attributed to the intense band system of perylene aggregates while the intensities of visible region peaks (437 and 465 nm) increased confirming the formation of PeNPs (Figure 2a). Strong emission peaks around 483 and 513 nm (Figure 2b) originated from free exciton states of quasi-spherical PeNPs in the PL emission spectrum also established the formation of PeNPs.

3.1. FT-IR Analysis

FT-IR spectra of NR₅₂₀ and PNR₅₂₀ are shown in Figure 3. The bands observed at 1637 and 3340 cm⁻¹ are due to bending and stretching vibrations of the -OH group of chemisorbed/physisorbed water molecules on TiO₂ surface [19]. The presences of sharp signals in the range of 600–1000 cm⁻¹ are typical for the O-Ti-O vibrations in TiO₂ [20]. The bands at 795 and 3340 cm⁻¹ are blue shifted to 801 and 3378 cm⁻¹, respectively, while the bands at 962 and 1637 cm⁻¹ are slightly red shifted to 952 and 1630 cm⁻¹, respectively, in PNR₅₂₀. The shifts in absorption peaks indicate the direct interaction of PeNPs with TiO₂ nanorods. In PNR₅₂₀, four additional peaks at 1348, 1476, 2852, and 2922 cm⁻¹ were observed and are due to C-N, C=O, and C-H stretching vibrations of perylene [20] confirming the presence of PeNPs in PNR₅₂₀.

3.2. XRD Analysis

The powder XRD patterns of HT, HT₄₂₀, NR₅₂₀, and PNR₅₂₀ in the range 20°–60° are shown in Figure 4. The samples, HT and HT₄₂₀, show diffraction peaks corresponding to hydrogen titanate of the formula H₂Ti₅O₁₁·3H₂O [JCPDF no: 44-0131]. H₂Ti₅O₁₁ is thermally unstable and as the calcination temperature increases, the peaks belong to hydrogen titanate phase disappear and the anatase phase TiO₂ [JCPDS no: 21-1272] becomes the main crystal form [8,9]. A decrease of the interlayer spacing occurs mainly due to the dehydration of interlayered OH groups [21]. XRD patterns demonstrate that both NR₅₂₀ and PNR₅₂₀ consist of pure anatase phase TiO₂. There were no peaks corresponding to PeNPs in the XRD spectrum of PNR₅₂₀ and may be due to the low amount of PeNPs used for modification. Crystallite sizes of the prepared samples were estimated using Scherrer's equation; $D_{\text{XRD}} = 0.9 \lambda / \beta \cos \theta$, where D is the crystallite size, λ is the

wavelength of X-ray used ($\lambda=0.15418$ nm), β and θ are full width at half maximum intensity (FWHM) (in radian) of XRD diffraction lines and half diffraction angle 2θ , respectively, and are given in Table 1. Compared to HT, crystallite size of HT₄₂₀ was decreased (9.04–7.5) attributed to the increase in FWHM with increasing calcination temperature resulted in the breaking of titanate nanostructures [21]. There was an increase in crystallite size of samples observed as calcination temperature increased from 420 to 520°C. The decrease of the FWHM with increasing calcination temperature could be due to the coalescences of grains at higher temperatures thus leading to increase in the average crystallite size due to improvement of crystallinity of nanostructures [22].

3.3. Morphological Analysis

Morphology of NR₅₂₀ was studied using HR-TEM analysis (Figure 5a-c) and the result shows that NR₅₂₀ exists as nanorods. These nanorods were not interconnected and are randomly oriented. Figure 5c shows the lattice fringes of NR₅₂₀ with d-spacing of 0.33 nm which confirms the single crystalline nature of nanorods. These results clearly confirm that NR₅₂₀ nanorods have pure anatase phase single crystalline structure grown along (101) direction, which is in good agreement with XRD results.

3.4. Diffuse Reflectance Spectra Analysis

The optical properties of the samples were studied using UV-Vis diffuse reflectance spectroscopy (DRS) and the results are shown in Figure 6. All samples exhibit the characteristic absorption band around 400 nm attributed to the intrinsic transition from the valence band to the CB of the nanostructured TiO₂ [23]. The absorption band edges of HT, HT₄₂₀, and NR₅₂₀ are 439, 433, and 400 nm, respectively. As the calcination temperature increases, the absorption edges show blue shift attributed to the differences in the surface nanostructures along with increase in crystallite size [23]. Titanate nanostructures (HT, HT₄₂₀)

Table 1: Crystallite size of synthesized samples.

Sample	Crystallite size (nm)
HT	9.04
HT ₄₂₀	7.5
NR ₅₂₀	16.10
PNR ₅₂₀	16.23

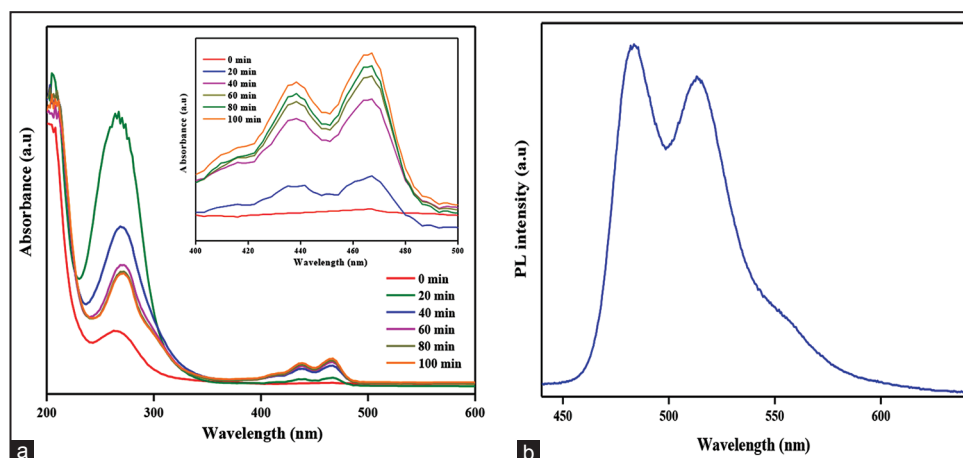


Figure 2: (a) Ultra violet-vis absorption spectra of perylene nanoparticles suspension at different time intervals (inset shows the enlarged view of absorption spectra in the range 400–500 nm) and (b) emission spectrum of PeNPs suspension at an excitation wavelength of 380 nm (Jesty et al., 2017).

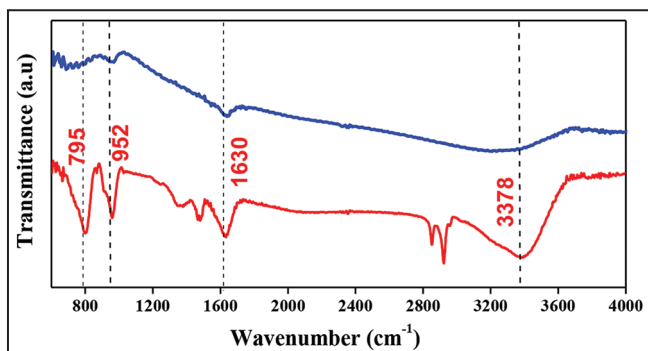


Figure 3: Fourier-transform infrared spectra of (a) NR₅₂₀ and (b) PNR₅₂₀.

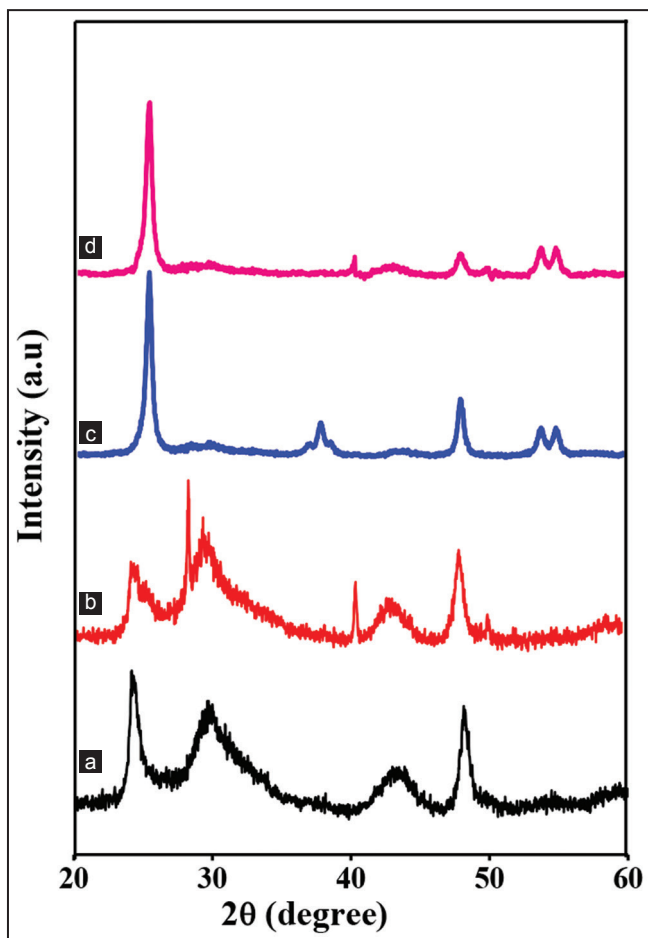


Figure 4: X-ray diffraction patterns of (a) HT, (b) HT₄₂₀, (c) NR₅₂₀, and (d) PNR₅₂₀.

show low band gap values ascribed to their hybrid structures [24]. Addition of PeNPs to NR₅₂₀ resulted in the red shift of absorption edge of NR₅₂₀ (400 nm–453 nm). PNR₅₂₀ shows shoulder peaks at 408, 437, and 470 nm and the peaks at 408 and 437 nm are attributed to the perylene monomers [25]. The $\nu=0 \rightarrow \nu'=1$ transition shown by perylene containing compounds was observed at 470 nm [26]. The band gaps (E_g , eV) of the samples were calculated using the equation, $E_g = 1239.8/\lambda$ where λ is the wavelength (nm) of absorption edges in the spectrum and are given in Table 2.

The nature of the band gap (either an indirect or direct transition) was determined using the power expression, $(\alpha h\nu)^n = K_{i,d}(h\nu - E_g)$, where E_g is the band gap energy, α is the absorbance, $h\nu$ is the absorption

Table 2: Band gap values of synthesized samples.

Samples	Band gap value obtained from $E_g = 1239.8/\lambda$ (in eV)	Band gap value obtained from $(\alpha h\nu)^2$ against $h\nu$ plot (in eV)
HT	2.82	2.83
HT ₄₂₀	2.86	2.86
NR ₅₂₀	3.10	3.10
PNR ₅₂₀	2.73	2.73

energy, and $K_{i,d}$ is the absorption constant for an indirect (subscript i) or direct (subscript d) transition corresponding to 1/2 and 2 for n , respectively [21]. Figure 7 shows the plots of $(\alpha h\nu)^2$ against photon energy $h\nu$ (eV) and the band gap energies are in agreement with onset energy observed in the absorption spectra confirming that the band gap is attributed to the direct transition. The lower band gap energy along with significant red shift of absorption edge in PNR₅₂₀ compared with NR₅₂₀ is due to the presence of photosensitive PeNPs, which subsequently results in the efficient utilization of sunlight.

3.5. Photoluminescence Spectra Analysis

PL spectra were used to investigate the efficiency of charge carrier trapping, migration, transfer, and the fate of photo-induced electrons and holes in the semiconductor. Room temperature PL emission spectra of HT, HT₄₂₀, NR₅₂₀, and PNR₅₂₀ at an excitation wavelength of 300 nm are shown in Figure 8. All samples show peaks in the range 420–430 and 460–470 nm. The broad peak at 420–430 nm is arising from band edge free excitons while one at 460–470 nm is resulting from binding excitons [27]. Calcinated samples HT₄₂₀ and NR₅₂₀ showed lower PL intensities compared to HT indicating the reduced recombination rate of photo-induced charge carriers under visible light irradiation. PNR₅₂₀ shows weaker emission intensity compared to NR₅₂₀, ascribed to the efficient separation of photogenerated charge carriers and the peaks observed in the range 445–500 nm are due to the emission from the free excited states of quasi spherical PeNPs [18].

3.6. Photocatalytic Activity Studies

Photocatalytic efficiencies of as-synthesized photocatalysts were evaluated by monitoring the photocatalytic degradation of RhB (25 ml of 15 ppm) under sunlight and results are shown in Figure 9. It is clear from the figure that the degradation of RhB without any photocatalyst is negligible which confirms that the decolorization of RhB dye takes place only by photocatalysis and not by photosensitization [28]. As the calcination temperature of samples is increased, rate of RhB degradation was increased implying the effect of calcination temperature on photocatalysts. TiO₂ nanorods modified by PeNPs (PNR₅₂₀) exhibited efficient photocatalytic activity compared to other samples and most active commercial photocatalyst, Degussa P25. The order of photocatalytic activity of synthesized samples was in the order, HT < HT₄₂₀ < NR₅₂₀ < Degussa P25 < PNR₅₂₀. PNR₅₂₀ shows the highest photocatalytic activity and gave complete degradation of RhB within 60 min of solar irradiation. It is reported that the degradation of RhB dye molecules occurs either through the cleavages of all-conjugated structures or through N-de-ethylation [29]. In this study, the degradation is through the cleavage of conjugated structures as the absorption peak position of RhB dye, remains constant with decrease in intensity with respect to time, as shown in Figure 9 (inset) [29].

Photocatalytic degradation of phenolic compounds such as 4-CP, R, and SA, the common endocrine disruptors usually found in the waste waters of industries, was studied using NR₅₂₀, PNR₅₂₀, and Degussa P25 and results are depicted in Figure 10. Photocatalytic degradation

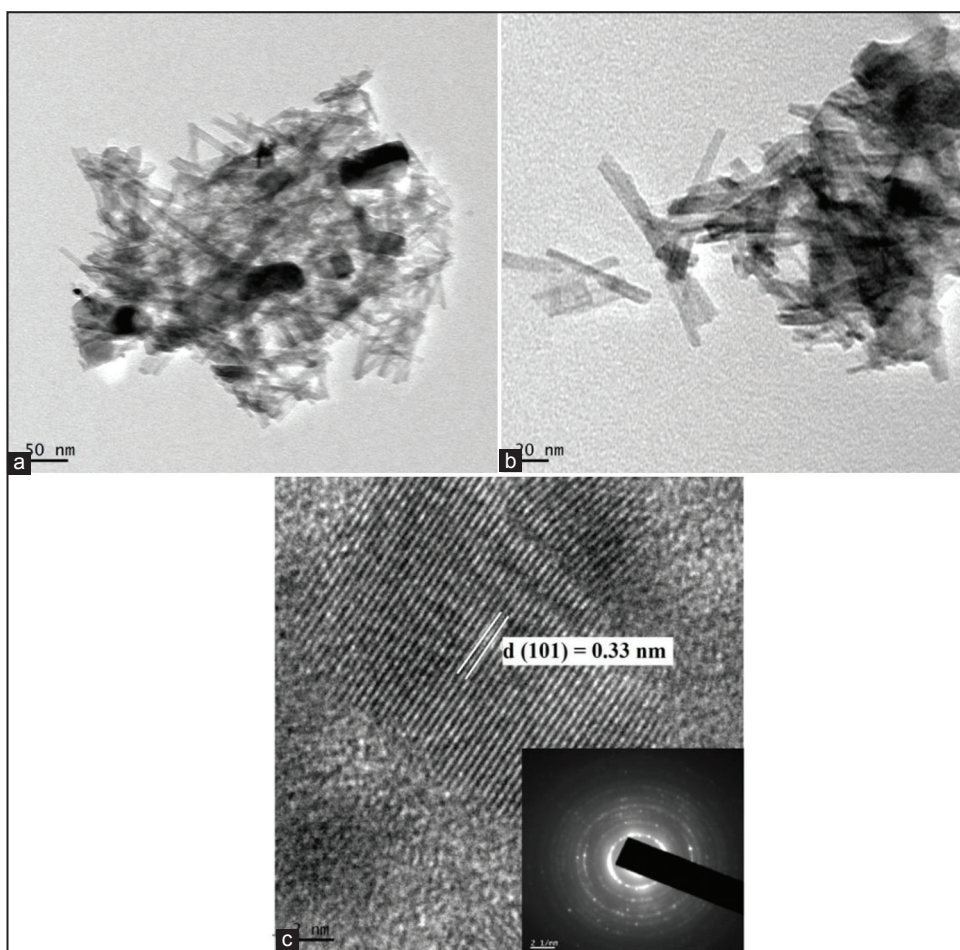


Figure 5: High resolution transmission electron microscopic images of NR₅₂₀.

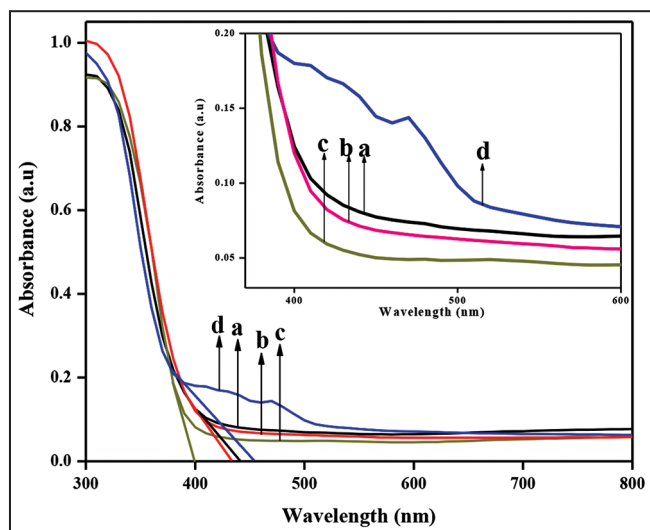


Figure 6: Diffuse reflectance spectroscopy (DRS) spectra of (a) HT, (b) HT₄₂₀, (c) NR₅₂₀, and (d) PNR₅₂₀ (inset shows the enlarged view of DRS spectra in the range 370–600 nm).

efficiency of PNR₅₂₀ was found to be greater than both NR₅₂₀ and Degussa P25. PNR₅₂₀ shows high photocatalytic efficiency attributed to the cooperative effect between TiO₂ and PeNPs. PNR₅₂₀ was able to completely degrade 4-CP, R, and SA within 100, 60, and 80 min of solar irradiation, respectively. When R was irradiated with sunlight in the presence of the photocatalysts, formation of colored intermediates

such as trihydroxy benzenes was indicated by slow color change of R suspension from white to brown [30]. The intensity of brown color was increased up to 40 min of solar light irradiation and was then decreased as the intermediates are converted to CO₂ and H₂O [30]. This study proves that PNR₅₂₀ can be used for the photocatalytic degradation of real life hazardous materials under sunlight.

It is well-known that active species such as hydroxyl radical ($\cdot\text{OH}$), superoxide anion radical ($\cdot\text{O}_2^-$), and hole (h^+) play significant role in the photocatalytic degradation of pollutants. To investigate the role of these active species during photocatalysis, various active species scavengers were used. Here, IPA [31], AA, and TEOA [32] were employed as the scavengers for hydroxyl free radicals ($\cdot\text{OH}$), superoxide anion radicals ($\cdot\text{O}_2^-$), and holes (h^+), respectively. Results (Figure 11) illustrate the influence of active species scavengers on the degradation of RhB under solar light irradiation. A significant suppression of photocatalytic activity is seen after the addition of IPA, AA, and TEOA, confirming the essential roles of hydroxyl free radicals ($\cdot\text{OH}$), superoxide anion radicals ($\cdot\text{O}_2^-$), and holes (h^+), respectively, in the photodegradation process. Thus, photocatalytic degradation of RhB dye by PNR₅₂₀ is governed by $\cdot\text{OH}$, $\cdot\text{O}_2^-$, and h^+ .

These observations would support the mechanism of pollutant degradation using PNR₅₂₀ and are shown in Figure 12. When PNR₅₂₀ was irradiated by sunlight, PeNPs get excited (PeNPs*) and the rapid electron (e^-) transfer occurs between PeNPs* and TiO₂ [Eqs. (1) - (2)]. The estimated reduction potential of perylene is -1.68 eV vs. NHE [33] which is sufficiently negative than that of CB edge of TiO₂ [-0.98 eV vs. NHE] [34] indicating that the electron transfer from PeNPs* to TiO₂ is favorable thermodynamically. Hence, the

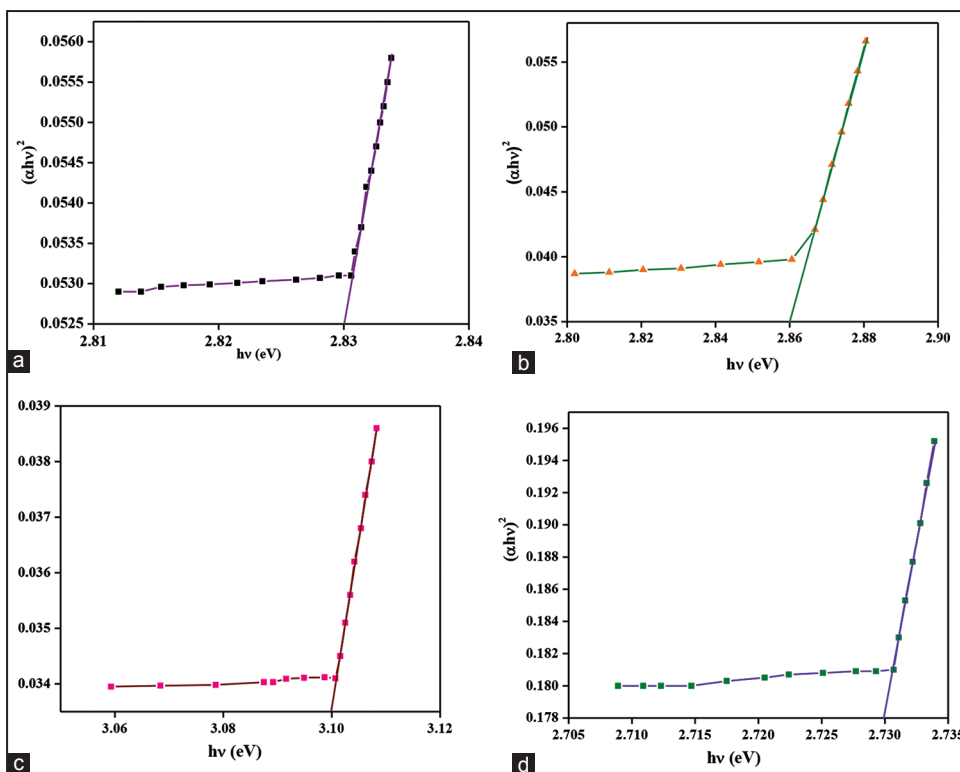


Figure 7: $(ah\nu)^2$ versus $h\nu$ plots of (a) HT, (b) HT₄₂₀, (c) NR₅₂₀ and (d) PNR₅₂₀.

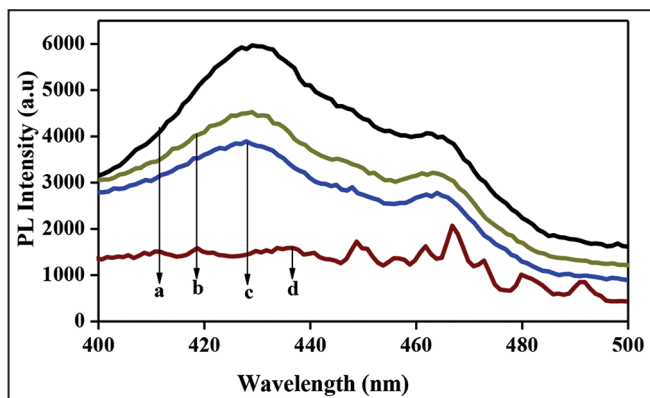


Figure 8: Room temperature photoluminescence emission spectra of (a) HT, (b) HT₄₂₀, (c) NR₅₂₀ and (d) PNR₅₂₀.

adsorbed PeNPs* can inject its e⁻ to the CB of TiO₂. Molecular oxygen in ambient atmosphere scavenges electrons from the CB of TiO₂ to produce superoxide (⁻O₂) radicals [Eq. (3)]. The charges would subsequently transform to the surface of the photocatalyst to react with water and dissolved oxygen to generate ⁻O₂ and hydroxyl (⁻OH) radicals or interact with pollutants directly. ⁻OH is also formed when the photogenerated electrons react with protons and dissolved oxygen (O₂) [Eqs. (4) - (7)]. The radicals were able to oxidize the pollutant molecules into CO₂ and H₂O due to their high oxidative capacity. The photogenerated charge carriers [holes (h⁺) and electrons (e⁻)], ⁻O₂ and ⁻OH radicals thus formed are mainly responsible for the degradation of pollutants through its successive attacks through formation of several intermediate products. The overall interfacial charge transfer reaction may be summarized as

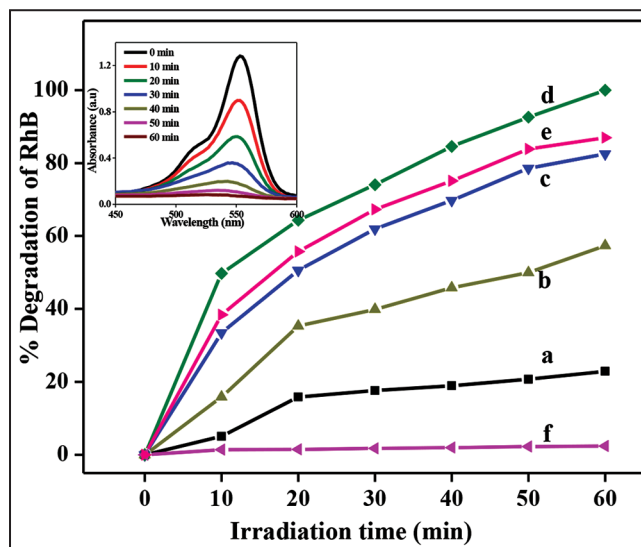
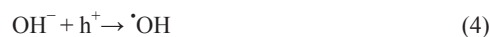


Figure 9: Photocatalytic degradation of rhodamine B (RhB) by (a) HT, (b) HT₄₂₀, (c) NR₄₂₀, (d) PNR₅₂₀, (e) Degussa P25, (f) RhB alone (inset shows ultra violet-vis absorption spectra of the time dependent photodegradation of RhB dye in the presence of PNR₅₂₀).



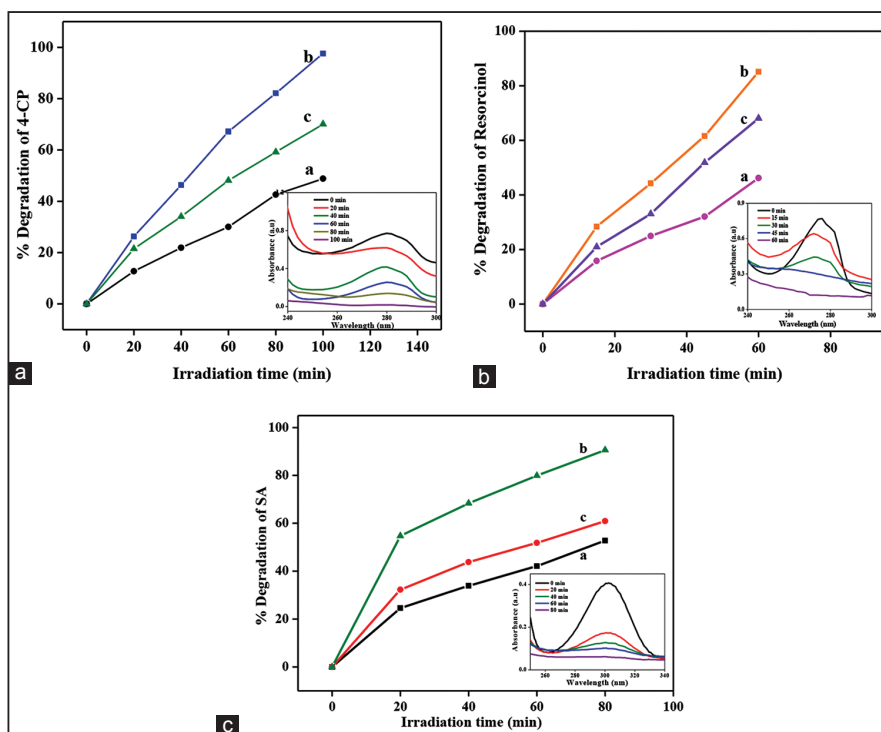


Figure 10: Photocatalytic degradation of (A) 4-chlorophenol, (B) resorcinol, and (C) salicylic acid by (a) NR₅₂₀, (b) PNR₅₂₀, and (c) Degussa P25 (inset shows Ultra violet-vis absorption spectra of the time dependent photodegradation of corresponding pollutants in the presence of PNR₄₂₀).

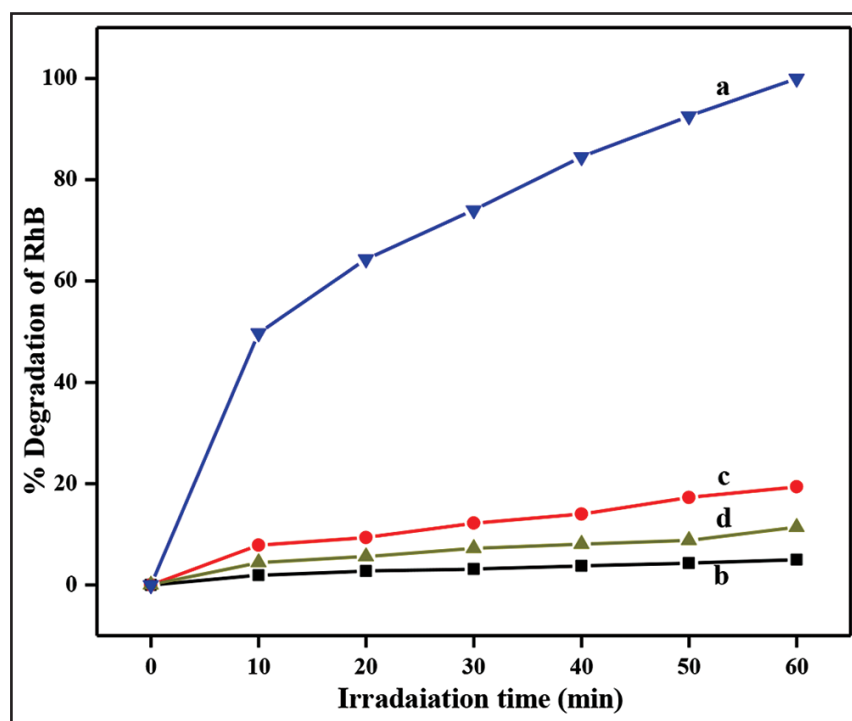


Figure 11: Photocatalytic degradation of rhodamine B by (a) PNR₅₂₀ alone, (b) PNR₅₂₀-AA, (c) PNR₅₂₀-IPA, and (d) PNR₅₂₀-triethanolamine.

3.7. Recycling Capacity of the Catalyst

For the assessment of stability and reusability of the synthesized photocatalyst, PNR₅₂₀ was used for the degradation of different solutions of RhB in four consecutive experiments while keeping the same reaction conditions (0.03 g catalyst + 25 ml of 15 ppm RhB, and

60 min of solar irradiation). Catalyst was recovered by centrifugation after each experiment and before next experiment; it was dried in an air oven and powdered well. Photocatalysts retain their high catalytic activity after being recycled 4 times, as shown in (Figure 13a and b) presents the FT-IR spectra of the PNR₅₂₀ photocatalyst before and after

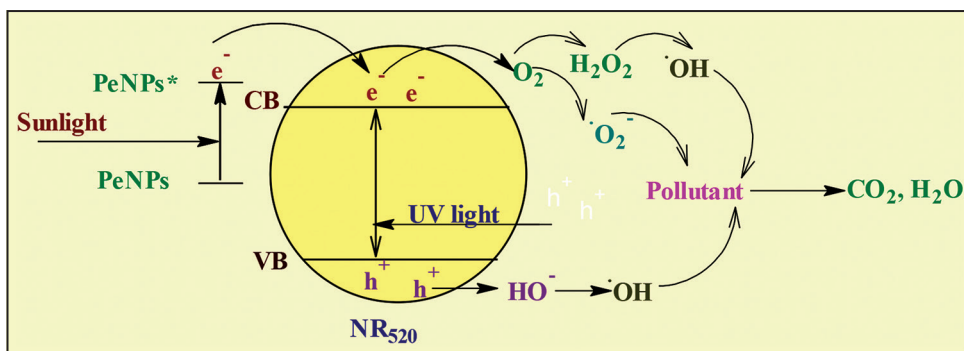


Figure 12: Mechanism of pollutant degradation using PNR₅₂₀ under solar light.

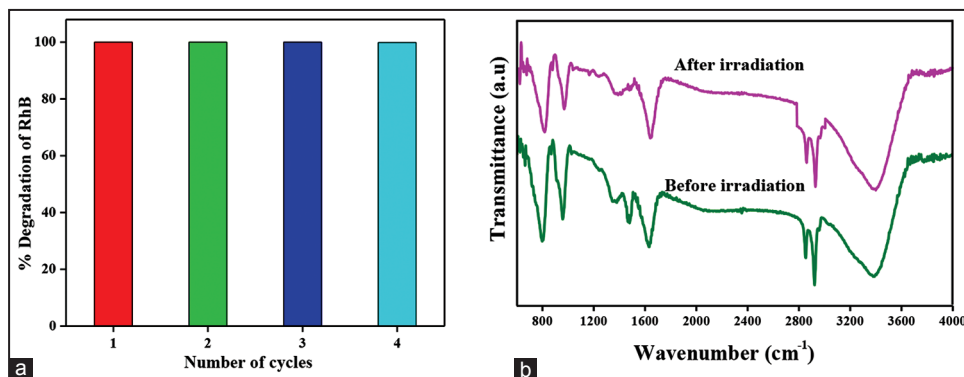


Figure 13: (a) Cyclic runs of PNR₅₂₀ for the degradation of RhB under solar irradiation and (b) Fourier-transform infrared spectra of PNR₅₂₀ photocatalyst before and after 4 cyclic runs.

four recycling runs for the photocatalytic degradation of RhB under solar irradiation. It is evident from FT-IR spectra that the spectrum of the recycled photocatalyst after photodegradation reactions was same as that of the fresh photocatalyst. These results indicate that PNR₅₂₀ has high chemical stability and is recoverable and reusable.

4. CONCLUSIONS

TiO₂ nanorods modified with PeNPs (PNR₅₂₀) showing high photocatalytic activity under sunlight were synthesized. TiO₂ nanorods were prepared through simple hydrothermal route, followed by calcination without using any templates. PeNPs were synthesized using GAH which acted both as reducing and stabilizing agent. DRS analysis showed that the addition of PeNPs red shifted the absorption edge of TiO₂ from 400 nm to 453 nm, resulting in the reduction of bandgap from 3.10 to 2.73 eV. HR-TEM analysis revealed that the synthesized anatase TiO₂ exists as nanorods. TiO₂ nanorods modified with PeNPs (PNR₅₂₀) could degrade common endocrine disruptors such as 4-CP, R, and SA and are superior photocatalysts than the most active commercial photocatalyst, Degussa P25. Active species scavenging experiment showed that $\cdot\text{OH}$, O_2^- , and h^+ are responsible for the degradation of pollutants. This study reveals that the incorporation of photosensitive organic nanoparticles like PeNPs to TiO₂ significantly enhances its visible light absorption and consequently improves its photocatalytic efficiency under solar light.

5. ACKNOWLEDGMENT

This work was financially supported by Kerala State Council for Science, Technology and Environment (KSCSTE) which is an autonomous institution of Science and Technology Department of Government of Kerala.

6. REFERENCES

- S. A. Bakar, C. Ribeiro, (2016) Rapid and morphology controlled synthesis of anionic S-doped TiO₂ photocatalysts for the visible-light-driven photodegradation of organic pollutants, *RSC Advances*, **6**: 36516-36527.
- Z. Liu, Y. Kanjo, S. Mizutani, (2009) Removal mechanisms for endocrine disrupting compounds (EDCs) in wastewater treatment physical means, biodegradation, and chemical advanced oxidation: A review, *Science of Total Environment*, **407**: 731-748.
- T. Jesty, S. Radhika, Y. Minjoong, (2016) Nd³⁺-doped TiO₂ nanoparticles incorporated with heteropoly phosphotungstic acid: A novel solar photocatalyst for degradation of 4-chlorophenol in water, *Journal of Molecular Catalysis A: Chemical*, **411**: 146-156.
- S. K. Pardeshi, A. B. Patil, (2009) Effect of morphology and crystallite size on solar photocatalytic activity of zinc oxide synthesized by solution free mechanochemical method, *Journal of Molecular Catalysis A: Chemical*, **308**: 32-40.
- Y. Zhu, M. W. Shah, C. Wang, (2017) Insight into the role of Ti³⁺ in photocatalytic performance of shuriken-shaped BiVO₄/TiO₂-x heterojunction, *Applied Catalysis B: Environmental*, **203**: 526-532.
- S. Ghasemi, S. J. Hashemian, A. A. Alamolhoda, I. Gocheva, S. R. Setayesh, (2017) Plasmon enhanced photocatalytic activity of Au@TiO₂-graphene nanocomposite under visible light for degradation of pollutants, *Materials Research Bulletin*, **87**: 40-47.
- X. Zhou, J. Lu, J. Jiang, X. Li, M. Lu, G. Yuan, Z. Wang, M. Zheng, H. J. Seo, (2014) Simple fabrication of N-doped mesoporous TiO₂ nanorods with the enhanced visible light photocatalytic activity, *Nanoscale Research Letters*, **9**: 34-41.

8. Y. Liu, Z. Wang, W. Wang, W. Huang, (2014) Engineering highly active TiO₂ photocatalysts via surface-phase unction strategy employing a titanate nanotube precursor, *Journal of Catalysis*, **310**: 16-23.
9. M. Rutar, N. Rozman, M. Pregelj, C. Bittencourt, R. C. Korošec, A. S. Škapin, A. Mrzel, S. D. Škapin, P. Umek, (2015) Transformation of hydrogen titanate nanoribbons to TiO₂ nanoribbons and the influence of the transformation strategies on the photocatalytic performance, *Beilstein Journal of Nanotechnology*, **6**: 831-844.
10. S. Kathirvel, C. Su, Y. J. Shiao, Y. F. Lin, B. R. Chen, W. R. Li, (2016) Solvothermal synthesis of TiO₂ nanorods to enhance photovoltaic performance of dye-modified solar cells, *Solar Energy*, **132**: 310-320.
11. L. Song, X. Zhao, L. Cao, J. W. Moon, B. Gu, W. Wang, (2015) Synthesis of rare earth doped TiO₂ nanorods as photocatalysts for lignin degradation, *Nanoscale*, **7**: 16695-16703.
12. S. Lai, W. Zhang, F. Liu, C. Wu, D. Zeng, Y. Sun, Y. Xu, Y. Fang, W. Zhou, (2013) TiO₂ nanotubes as animal drug delivery system and *in vitro* controlled release, *Journal of Nanoscience and Nanotechnology*, **13**: 91-107.
13. C. F. Chang, C. Y. Man, (2014) Magnetic photocatalysts of copper phthalocyanine-sensitized titania for the photodegradation of dimethyl phthalate under visible light, *Colloids and Surfaces A: Physicochemical and Engineering Aspects*, **441**: 255-261.
14. T. Hasobe, S. Hattori, P. V. Kamat, Y. Urano, N. Umezawa, T. Nagano, S. Fukuzumi, (2005) Organization of supramolecular assemblies of fullerene, porphyrin and fluorescein dye derivatives on TiO₂ nanoparticles for light energy conversion, *Chemical Physics*, **319**: 243-252.
15. L. N. Nguyen, S. K. Pradhan, C. N. Yen, M. C. Lin, C. H. Chen, C. S. Wu, K. S. C. Liao, M. T. Lin, C. D. Chen, (2013) High performance phototransistors based on single crystalline perylene tetracarboxylic dianhydride nanoparticle, *Applied Physics Letters*, **103**: 183301-183305.
16. P. B. Dhanaji, B. K. Govind, M. G. Kalyanrao, R. P. Shivajirao, (2013) Cetyltrimethylammonium bromide stabilized perylene nanoparticles for fluorometric estimation of bicarbonate anion: Spectroscopic approach, *Analytical Methods*, **5**: 5324-5330.
17. L. Kang, Z. Wang, Z. Cao, Y. Ma, H. Fu, J. Yao, (2007) Colloid chemical reaction route to the preparation of nearly monodispersed perylene nanoparticles: Size tunable synthesis and three-dimensional self organization, *Journal of American Chemical Society*, **129**: 7305-7312.
18. T. Jesty, S. Radhika, Y. Minjoong, (2017) Graphitic carbon nitride modified with perylene nanoparticles as efficient solar photocatalyst, *Molecular Catalysis*, **433**: 274-281.
19. S. A. Bakar, G. Byzynski, C. Ribeiro, (2016) Synergistic effect on the photocatalytic activity of N-doped TiO₂ nanorods synthesized by novel route with exposed (110) facet, *Journal of Alloys and Compounds*, **666**: 38-49.
20. A. Senthilraja, B. Krishnakumar, M. Swaminathan, S. Nagarajan, (2014) Self-assembly, photophysical and electrochemical properties and activation of the TiO₂ photocatalyst by perylene bisimides, *New Journal of Chemistry*, **38**: 1573-1580.
21. R. Yoshida, Y. Suzuki, S. Yoshikawa, (2005) Effects of synthetic conditions and heat-treatment on the structure of partially ion-exchanged titanate nanotubes, *Materials Chemistry and Physics*, **91**: 409-416.
22. G. H. Mhlongo, D. E. Motaung, S. S. Nkosi, H. C. Swart, G. F. Malgas, K. T. Hillie, B. W. Mwakikung, (2014) Temperature dependence on the structural, optical and paramagnetic properties of ZnO nanostructures, *Applied Surface Science*, **293**: 62-70.
23. B. Santara, P. K. Giri, (2013) Impact of reaction temperature, stirring and cosolvent on the solvothermal synthesis of anatase TiO₂ and TiO₂/titanate hybrid nanostructures: Elucidating the growth mechanism, *Materials Chemistry and Physics*, **137**: 928-936.
24. H. Yu, J. Yu, B. Cheng, M. Zhou, (2006) Effects of hydrothermal post treatment on microstructures and morphology of titanate nanoribbons, *Journal of Solid State Chemistry*, **179**: 349-354.
25. D. Oliveira, K. Baba, J. Mori, Y. Miyashita, H. Kasai, H. Oikawa, H. Nakanishi, (2010) Using an organic additive to manipulate the sizes of perylene nanoparticles, *Journal of Crystal Growth*, **312**: 431-436.
26. C. Xue, Y. Xue, L. Dai, A. Urbas, Q. Li, (2013) Size and shape dependent fluorescence quenching of gold nanoparticles on perylene dye, *Advanced Optical Materials*, **175**: 1-7.
27. Q. Xiao, Z. Si, Z. Yu, G. Qiu, (2007) Sol-gel auto combustion synthesis of samarium doped TiO₂ nanoparticles and their photocatalytic activity under visible light irradiation, *Materials Science and Engineering B*, **137**: 189-194.
28. M. Quasim, K. Asghar, B. R. Singh, S. Prathapani, W. Khan, A. H. Naqvi, (2015) Magnetically recyclable Ni_{0.5}Zn_{0.5}Fe₂O₄/Zn_{0.95}Ni_{0.05}O nano photocatalyst: Structural, optical, magnetic and photocatalytic properties, *Spectrochimica Acta Part A: Molecular and Biomolecular Spectroscopy*, **137**: 1348-1356.
29. K. Sridharan, T. Kuriakose, R. Philip, T. J. Park, (2014) Transition metal (Fe, Ni and Co) oxide nanoparticles grafted graphitic carbon nitrides as efficient optical limiters and recyclable photocatalysts, *Applied Surface Science*, **308**: 139-147.
30. A. B. Patil, K. R. Patil, S. K. Pardeshi, (2010) Ecofriendly synthesis and solar photocatalytic activity of S-doped ZnO, *Journal of Hazardous Materials*, **183**: 315-323.
31. M. Jia, X. Hu, S. Wang, Y. Huang, L. Song, (2015) Photocatalytic properties of hierarchical BiOXs obtained via an ethanol assisted solvothermal process, *Journal of Environmental Science*, **35**: 172-180.
32. X. Zhang, L. Yu, C. Zhuang, T. Peng, R. Li, X. Li, (2014) Highly asymmetric phthalocyanine as a sensitizer of graphitic carbon nitride for extremely efficient photocatalytic H₂ production under near infrared light, *ACS Catalysis*, **4**: 162-170.
33. S. K. Lee, Y. Zu, A. Herrmann, Y. Geerts, K. Mullen, A. J. Bard, (1999) Electrochemistry, spectroscopy and electrogenerated chemiluminescence of perylene, terylene, and quaterylene diimides in aprotic solution, *Journal of American Chemical Society*, **121**: 3513-3520.
34. S. Chen, L. W. Wang, (2012) Thermodynamic oxidation and reduction potentials of photocatalytic semiconductors in aqueous solution, *Chemistry of Materials*, **24**: 3659-3666.

***Bibliographical Sketch**

Dr. Jesty Thomas is a faculty member of Research Department of Chemistry, Kuriakose Elias College, Mannanam and is an approved research guide of Mahatma Gandhi University. She received M.Sc degree from Mahatma Gandhi University, Kerala with second rank and obtained Ph.D from NIIST, C.S.I.R. Her postdoctoral research was at Chungnam National University, South Korea. She worked as scientist of Department of Science and Technology (WOS-A), India. She was also awarded 'Young Scientist Fellowship' (Fast Track Scheme) by Department of Science & Technology, India. She has more than 100 research publications (in journals and Conference proceedings). She was selected as "OUTSTANDING WOMAN IN SCIENCE" for the initiatives and developments in the field of Chemistry by Venus International Foundation in 2018. She also received "Research Excellence Award 2020" (ICSETS-2020).

Dr. Jesty presented several papers in National and International conferences including ten invited talks. She has been invited by United Scientific Group to discuss her research findings in "International Conference on Catalysis and Chemical Engineering 2017" held at USA. She has completed three major research projects funded by UGC/DST. Her research works received ten "Best Research Paper" awards. Her research group synthesized a new crystal structure and has been accepted by 'Cambridge crystallographic data center' (CCDC971490). She also received 'Best Teacher Award' from St. Joseph's College of Engineering and Technology, Pala.

She is a member of Editorial board of the international journal, "Materials Physics and Chemistry" and is the reviewer of articles of several international journals and received "Recognised Reviewer Status" from Elsevier and RSC publications. She served as thesis reviewer and external examiner for the award of Ph.D degree and also as expert member for "Revenue District Science Inspire Award". Dr. Jesty has membership in several academic bodies like Indian Society for Technical Education, Indian Science Congress, Kerala Science Academy, PG Board of Studies (Mahatma Gandhi University) etc. Her research interests include development of nanomaterials for solar photocatalysis, development of artificial photosynthetic systems and synthesis of luminescent inorganic-organic hybrid materials.



Dr. Radhika.S obtained her PhD in Chemistry (2018) from Mahatma Gandhi University, Kottayam, Kerala under the guidance of Dr. Jesty Thomas. She is currently working as Assistant Professor on contract at the Department of Chemistry, BCM College, Kottayam, Kerala. She has published four international and five national papers in highly peer reviewed journals